geoconvention
Virtual Event
September 13 - 15
2021

Fluid saturation and pressure changes in the Hugin Formation of the Volve oil field: Insights from time-lapse, rock physics, and pore pressure prediction

Draga Talinga and Carl Reine
Sound QI Solutions

Summary

In this study, we combined time-lapse seismic inversion and pore pressure estimates to predict changes in water saturation and pressure produced by water injection and depletion in the Hugin Formation of the Volve oil field, Central North Sea Basin. This deep reservoir is particularly challenging because of its thin nature, steep dips, compartmentalization from faulting, heterogeneous permeability structure, and an expected low-contrast between the velocities in oil- and water-saturated sandstones.

We determined the changes in reservoir elastic properties by subtracting the results obtained from the simultaneous inversion of the baseline and monitor data. A rock physics model using the reservoir properties was used to find relationships between changes in water saturation and pore pressure, and changes in the LambdaRho and Lambda/Mu elastic properties. We interpreted changes in water saturation using the observed changes in elastic properties and an equivalent rock-physics template. Pressure changes were estimated directly by relating changes in pore pressure to changes in effective stresses corresponding to the two datasets. The mapped water saturation changes suggest an increase in the saturation on the structural crest and around the location of known water injectors. The mapped pore-pressure differences correlate well with the location of water injectors and areas of expected depletion.

Time-lapse inversion

Variations in saturation or pore pressure produce changes in fluid compressibility and density, which in turn result in changes in the elastic properties of the bulk rock volume. Time-lapse seismic analysis identifies these changes from traveltime shifts and amplitude effects, which can then be used to quantify changes in impedance and density between baseline and monitor data.

Between the baseline and calibrated monitor surveys, large differences in amplitude are seen on the structural crest, where the producing wells are located (Figure 1). Additional minor differences, less than 10% change, are seen on the flanks of the structure, corresponding to the location of the water injectors. Properties from a simultaneous inversion further differentiate these areas, where P-wave velocity and density both increase on the structural high and decrease on the flanks. The simultaneous inversions of the baseline and monitor both used the same low-frequency model.

Estimation of saturation and pressure changes

Quantification of pressure and saturation changes during reservoir production is challenging due to the competing nature of these two effects. For example, both pressure depletion and increased water saturation are accompanied by an increase in seismic velocity. However, depending on the specific conditions, the velocity change is less sensitive to pore pressure than to saturation. Therefore, to understand the relationships between the time-lapse results and the expected

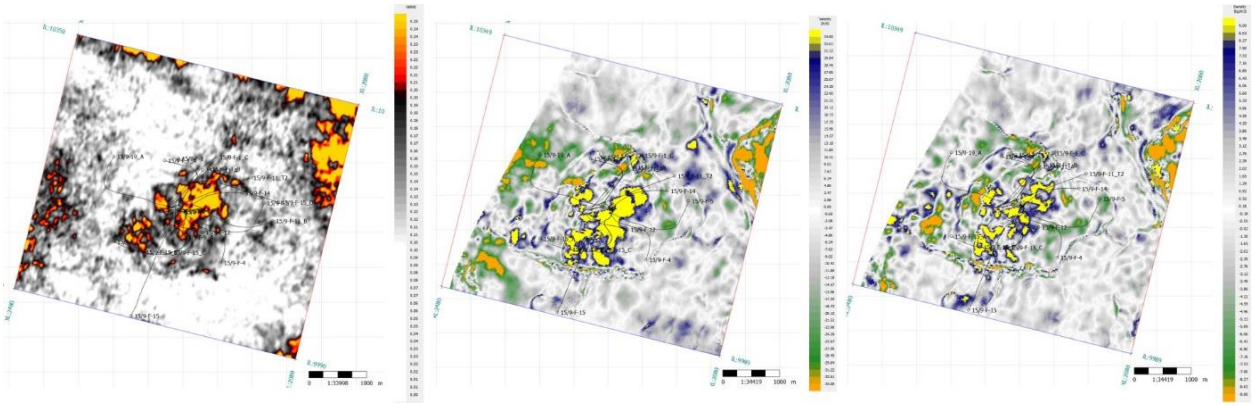

Figure 1. Normalized amplitude difference map between the calibrated monitor and baseline (left), and velocity (center) and density (right) differences obtained from the simultaneous inversion.

changes in reservoir saturation and pore pressure, we need to use rock-physics modelling.

1) Saturation Changes

For building the rock-physics model of the Hugin reservoir, we used a consolidated sandstone model (Vernik and Kachanov, 2010) to estimate the bulk and shear moduli of the dry sand. Gassmann fluid substitution (Mavko et al., 2020) was used to calculate the saturated moduli. After calibration with the log data, the rock-physics model was systematically changed to create templates that covered the range of mineralogy and porosity specified in the Well Discovery Report (Statoil, 1993).

The rock-physics analysis showed the theoretical magnitudes of the effects of water saturation and pressure changes on the elastic properties. In Lambda/Mu and LambdaRho crossplot space, the saturation effects are dominant, with pore-pressure effects requiring considerable pressure variations. As a result, this template was used only to interpret the saturation changes, but the difference in the two parameters' sensitivity helped dissociate their effects (Figure 2). The

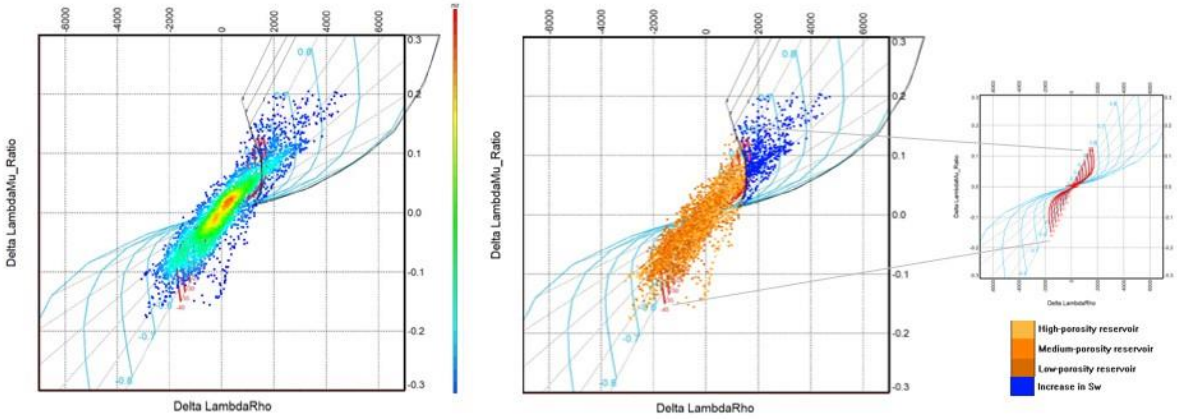

Figure 2. Crossplots to classify changes in water saturation. The rock-physics template is shown with unclassified (left) and classified seismic points (right), with porosity being previously classified. Blue curves are constant changes in saturation and red curves in the inset are constant changes in pore pressure. Grey lines represent constant porosities being modelled.

interpretation of water saturation changes (Figure 3) shows the lateral variation through the reservoir, with a good correlation between the increase in saturation and the position of the injection wells.

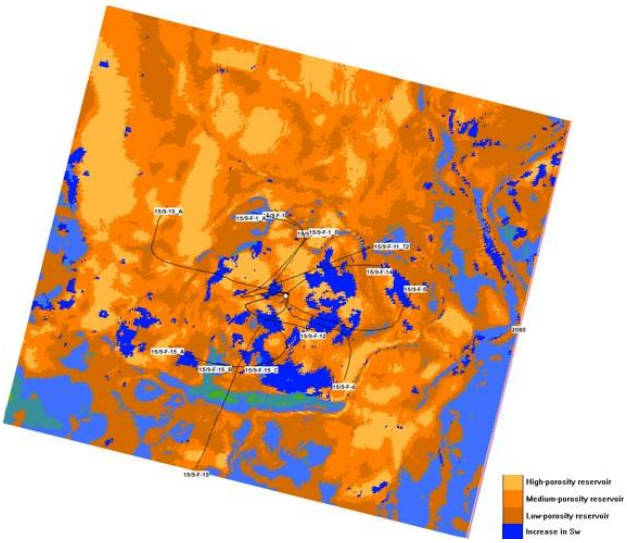

Figure 3. Classification showing the increase in water saturation (dark blue) around injectors 15/9-F-4 and 15/9-F-5. The slice is 8 ms above the base of the reservoir.

2) Pressure changes

We investigated the changes in pore pressure using two different methods. The first approach is using Eaton's method (Eaton, 1972), with the inverted density and P-wave velocity for the baseline and monitor as input. The application of the method for the Volve field, including lithology- and age-dependent normal-compaction trends, is described further by Talinga and Reine (2021). The magnitudes of pore pressure variations from this method are small and showed increased pore pressure up to 0.52 MPa on the northern and northeast flanks, and a slight decrease of 0.35 MPa on the crestal area (Figure 4, left).

The second approach to measuring pore-pressure changes used a workflow proposed by Landrø and Kvam (2002), relating the time-lapse changes in P-wave velocity to changes in pressure from the initial conditions. Their relationships are derived from the Hertz-Mindlin model for precompacted granular materials (Mindlin, 1949):

$$\frac{\Delta V_p}{V_{p\,base}} = \left(\frac{\sigma_{v\,eff\,mon}}{\sigma_{v\,eff\,base}}\right)^{\frac{1}{6}} - 1 \qquad (1)$$

where $V_{p\,base}$ is the baseline P-wave velocity of the reservoir, ΔV_p is the change in reservoir P-wave velocity between monitor and baseline surveys, and $\sigma_{v\,eff\,base}$ and $\sigma_{v\,eff\,mon}$ are the vertical effective stresses at the initial pressure and production conditions, respectively.

The vertical effective stress $\sigma_{v\,eff}$ is the stress component carried by the rigid rock matrix, and it is affected by the total vertical stress $\sigma_{v\,tot}$ imposed by the overlying rock column and by the internal pore pressure P_P within the matrix:

$$\sigma_{v\,eff} = \sigma_{v\,tot} - \alpha P_P \qquad (2)$$

where α is the effective stress coefficient, usually approximated with the Biot coefficient. The Biot coefficient estimated from rock physics modelling was 0.72. Total vertical stress is calculated by the integration of the bulk density over the full depth column. Rewriting Equation 1, we are able to obtain the P_P for the monitor conditions:

$$P_{P\,mon} = \frac{\sigma_{v\,tot\,mon} - \left(\frac{\Delta V_p}{V_{p\,base}}+1\right)^6 (\sigma_{v\,tot\,base} - \alpha P_{P\,base})}{\alpha} \qquad (3)$$

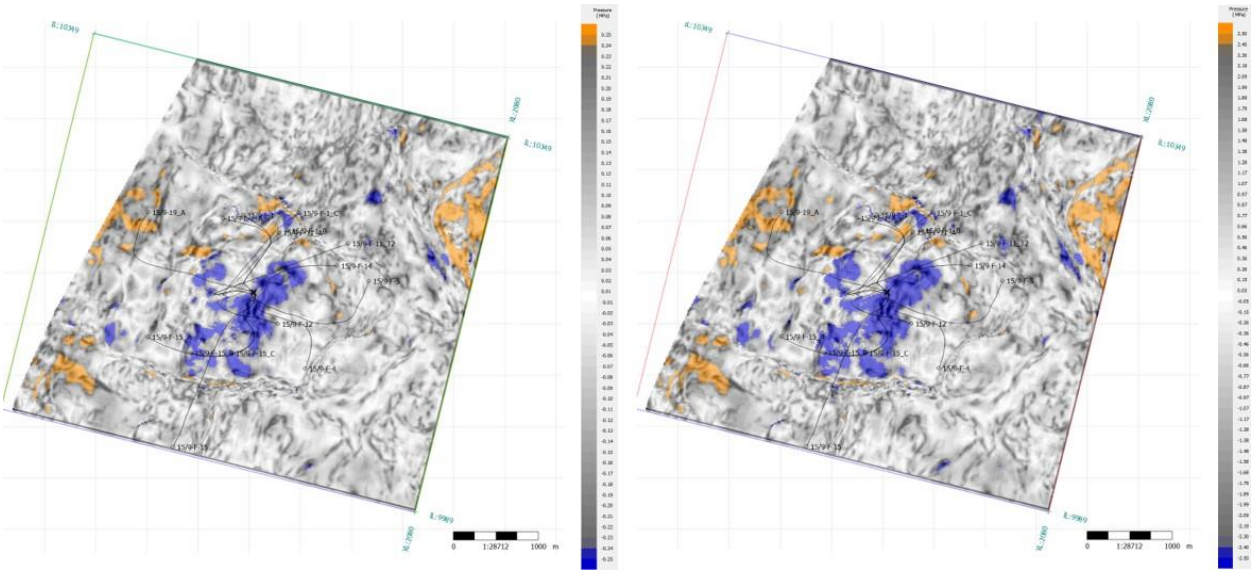

Figure 4. Average pore-pressure differences for the Hugin reservoir estimated using Eaton's method (left), and using the Landrø-Kvam approach. Superimposed discontinuity map shows pressure anomalies terminating against faults. The extent of pressure changes is similar, but there is a difference in the predicted ranges.

The exponent in Equation 1 can be calibrated using ultrasonic measurements on core or if monitor pressures are available. In the absence of both of these data options, we kept the theoretical value of 1/6. The pore pressure changes obtained from the Landrø-Kvam method indicate an increase in pore pressure of up to 4 MPa on the northern flank, 2 MPa on the northeast flank, and a decrease of up to 5.5 MPa on the structural high (Figure 4, right).

Uncertainty in the results comes primarily from the absence of monitor pressure data with which to calibrate the calculations. For Eaton's method, this requires that empirical parameters calculated from the baseline data. For the Landrø-Kvam method, the absence of monitor data prohibits the calibration of the equation exponent. There is also uncertainty from the consolidated nature of the Hugin reservoir compared to the unconsolidated Hertz-Mindlin assumption. Although there is a discrepancy in the magnitude of pressure changes estimated using the two methods, the overall interpretation of both is consistent. This is due to the fact that they both rely on changes in P-wave velocity. We used the pressure magnitudes from the Landrø-Kvam model to interpret pressure changes within the reservoir, updating the classified facies (Figure 6).

Conclusions

We tested a workflow for discriminating between saturation- and pore-pressure changes by integrating time-lapse inversion with rock-physics modelling and previously predicted baseline pore pressure. Results of rock-physics modelling showed that the elastic properties respond to fluids changing from oil to water, but they are less sensitive to changes in pressure. The difference in sensitivities allowed us to decompose the effects into saturation effects, interpreted from rock-physics modelling templates, and pressure effects, estimated using predicted pressure changes.

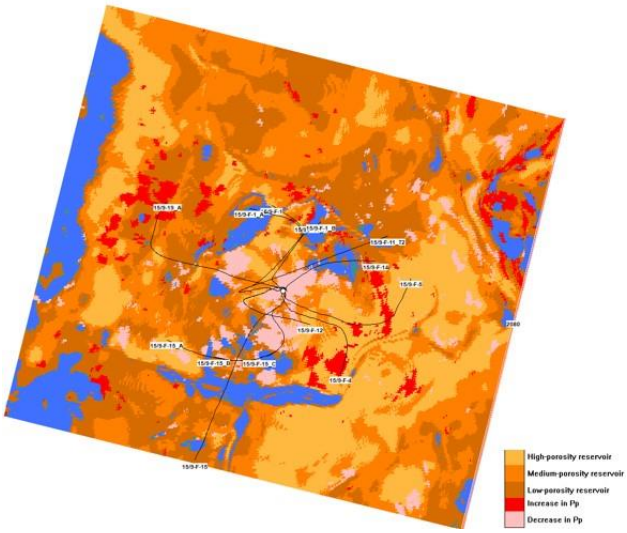

Figure 5. Estimated pore-pressure changes 8 ms below the top of the reservoir. Red and pink are increases and decreases in pore pressure, respectively. Increases in pressure correlate with locations of injectors, for example 15/9-F-4, 15/9-F-5, and 15/F-9-1_B.

The pore pressure for the monitor survey was estimated from the time-lapse inversion results, a theoretical velocity-effective stress relationship derived from the Hertz-Mindlin model, proposed by Landrø and Kvam (2002), and a previously predicted pore pressure model for the baseline (Talinga and Reine, 2021). We obtained two separate facies volumes corresponding to the saturation-change and pressure-change attributes and observed that most of the pressure decrease and saturation increase occur on the structural high without completely overlapping.

The interpretation shows an increase in water saturation on the structural crest, where oil is expected to be replaced by water, and at some of the known injector locations. These areas also predominantly show an increase in pore pressure. Decreasing pore pressure is indicated in areas where pressure depletion is expected. Furthermore, the boundaries of saturation and pressure anomalies correlate with trajectory of known faults. In absence of additional time-lapse information and core measurements, the results are not a definitive predictive model, but are useful to guide our understanding of the changes in this reservoir's saturation and pressure or in areas with similar complexities.

Acknowledgements

We would like to thank Equinor, ExxonMobil, Bayerngas, and Norwegian Petroleum Directorate for permission to use the Volve field dataset for research.

References

Biot, M. A., 1956. Theory of propagation of elastic waves in a fluid saturated porous solid. I. Low-frequency range: Journal of the Acoustical Society of America, 28, no. 2, 168–178, doi: 10.1121/1.1908239.
Dvorkin, J., & Nur, A. (1996). Elasticity of high-porosity sandstones: Theory for two North Sea data sets. Geophysics, 61, 1363-1370.
Eaton, B. A. (1972). The effect of overburden stress on geopressure prediction from well logs.
Journal of Petroleum Technology, 24(8), 929-934.
Landrø, M. and Ø. Kvam, 2002. Pore pressure estimation – what can we learn from 4D? Recorder, 27, no. 07.
Mindlin, R.D. 1949. Compliance of elastic bodies in contact. Journal of Applied Mechanics 16, 259–268.
Mavko, G., T. Mukerji, and J. Dvorkin, 2020. The rock physics handbook, Third edition, Cambridge University press.
Statoil. (1993). Discovery Evaluation Report, Well 15/9-19 SR, Theta Vest Structure.
Talinga, D. and C. Reine, 2021. Integrating Pore Pressure and Lithology Prediction from Well and Seismic Data to Characterize Abnormal Pressures in the Compartmentalized Volve Oil Field, Central North Sea, Recorder (In press).
Vernik, L., and M. Kachanov, 2010. Modeling elastic properties of siliciclastic rocks, Geophysics, 75, no. 6, E171-E182.